WILLIAM & MARY
CHARTERED 1693

Undergraduate Honors Theses

Theses, Dissertations, & Master Projects

7-2012

Global Dynamics of Pulse-Coupled Oscillators

Allison Leslie Corish
College of William and Mary

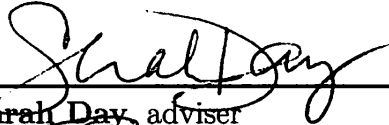Follow this and additional works at: https://scholarworks.wm.edu/honorstheses

Global Dynamics of Pulse-Coupled Oscillators

A thesis submitted in partial fulfillment of the requirement
for the degree of Bachelor of Science in Mathematics from
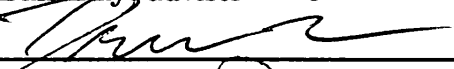The College of William and Mary
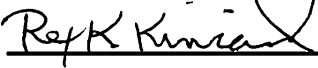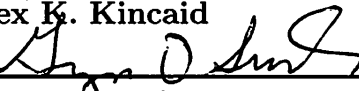
by

Allison Leslie Corish

Accepted for ___Honors___

_____
Sarah Day, adviser

_____
M. Drew LaMar, adviser

_____
Rex K. Kincaid

_____
Gregory D. Smith

Williamsburg, VA
April 26, 2012

Acknowledgements

Abstract

Networks of pulse-coupled oscillators can be used to model systems from firing neurons to blinking fireflies. Many past studies have focused on numerical simulations and locating the synchronous state of such systems. In this project, we construct a Poincaré map for a system of three pulse-coupled oscillators and use rigorous computational techniques and topological tools to study both synchronous and asynchronous dynamics. We present sample results, including the computed basin of attraction for the synchronous state as well as a depiction of gradient-like dynamics in the remainder of the phase space. In the future, we hope to automate this process so that it can be applied to a wide range of network topologies and parameter values.

Contents

List of Figures

Chapter 1

Introduction

Witnesses have observed that fireflies in regions of Thailand and the Great Smoky Mountains tend to synchronize their blinking. An individual firefly is an oscillator, blinking periodically over extended periods of time. A firefly spends most of its cycle in darkness, apart from a brief flash. When it does blink, it can influence other fireflies around it to either advance or delay the time of their next flash. In this sense, a firefly is more specifically a *pulse-coupled oscillator* since the stimulus that influences its neighbors is short in time relative to the period of oscillation. Whether or not a firefly is influenced by another is closely tied to proximity and line of sight. Mathematically, we record the allowed interactions as a network, or directed graph; each vertex corresponds to a firefly with a directed edge from vertex i to vertex j if the firing of firefly i influences firefly j. See Figure 1.1.

There are many interesting network topologies for systems of pulse-coupled oscillators. For example, if each firefly can be influenced by the firing of each other firefly, then this corresponds to a complete network where every vertex has a directed edge to every other vertex. See Figure 1.1 a). However, we may also be interested in the scenario where the blinking of certain fireflies influences only a subset of the population.

One natural question to ask at this point is "Will the fireflies synchronize their blinking?" The answer depends on network topology and the strength and type of coupling between the oscillators. Several previous studies focus on finding and characterizing synchronous behavior in coupled oscillator systems, often analyzing linear stability of the synchronous state [7, 9, 15, 13]. Most focus on a complete network and/or infinitely many oscillators and can be applied to systems of coupled oscillators from fireflies to neurons. Research in these areas has followed many paths and even given rise to a popular math book by Steven Strogatz called *Sync: The Emerging Science of Spontaneous Order* [11].

Two questions that motivate this work are "Can we study network topologies

a)   b)
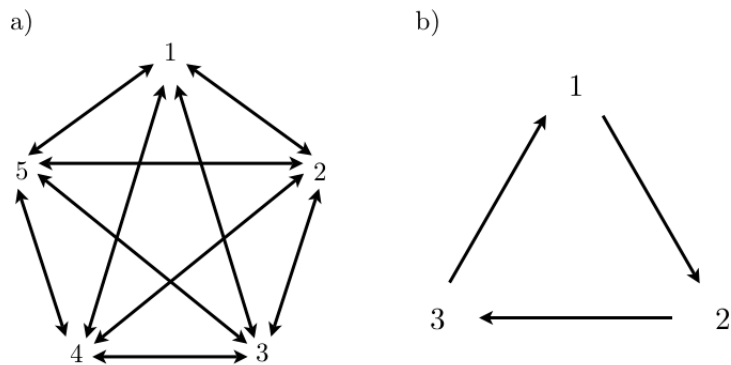
Figure 1.1: a) A complete directed network with five nodes; b) Our particular directed network with three nodes.

that are not complete?" and "Can we understand global dynamics rather than just local dynamics at the synchronous state?" With this in mind, we choose to study the directed cycle of three oscillators depicted in Figure 1.1 b). Numerical and analytical techniques such as linearization quickly break down because the model is discontinuous and its closed-form expression is complicated. For comparison with the numerical techniques that are the focus of this paper, we use linearization to analyze the stability of fixed points and point out the difficulties with this approach. Further analysis is performed in Chapter 3 to set the stage for expected results. In Chapter 4, we establish the mathematical theory necessary for building the rigorous computational approach. This approach is based on *Conley index theory*, a tool from algebraic topology that is well-suited for rigorous numerical computations. Finally, in Chapter 5, we present sample results for our chosen system of three pulse-coupled oscillators. These results include a computed basin of attraction for the synchronous state, asynchronous fixed points, and connecting orbits between them, giving a global picture of the dynamics. In the last section we discuss an approach for generalizing these techniques in order to study families of pulse-coupled oscillator systems with various network topologies and/or types and strengths of coupling.

Chapter 2

Defining the Network and Model

We begin the construction of our model with the definition of an *oscillator*. As motivation for such a definition, consider a simple pendulum composed of a bob of mass m suspended from a pivot by a rigid, weightless rod of length l. Let θ be the angle of displacement of the rod from the vertical, down position and let g be the constant for gravitational acceleration (see Figure 2.1). Assuming there is no friction, the equation for the motion of a pendulum can be derived using Newton's Second Law. Applied here, the law states that the force in the θ direction, $\frac{mg}{l}\sin\theta$, is equal to mass m times acceleration, $\frac{d^2\theta}{dt^2}$, in the θ direction. This yields the following governing equation for the system:

$$\frac{d^2\theta}{dt^2} + \frac{g}{l}\sin\theta = 0. \tag{2.1}$$

Equation (2.1) is a nonlinear, second-order differential equation. To simplify the equation, we assume a θ sufficiently small so that $\sin\theta \approx \theta$. This yields the approximate pendulum motion equation

$$\frac{d^2\theta}{dt^2} + \frac{g}{l}\theta = 0. \tag{2.2}$$

The general solution to (2.2) is $\theta(t) = C_1 \cos\left(\sqrt{\frac{g}{l}}t\right) + C_2 \sin\left(\sqrt{\frac{g}{l}}t\right)$, where C_1 and C_2 are constants determined by initial conditions. For example, given the initial conditions $\theta(0) = \frac{\pi}{2}$ and $\theta'(0) = 0$, we get the particular solution $\theta(t) = \frac{\pi}{2}\cos\left(\sqrt{\frac{g}{l}}t\right)$. See Figure 2.2. This is the kind of intrinsic frequency oscillator that we will deal with for the remainder of this project. In what follows, we will be primarily concerned with *phase* (i.e. the oscillator's location in time relative to its period), rather than time, as our independent variable. Our goal in studying phase is twofold. Firstly, studying an oscillator's phase is a convention we use to normalize the period to 1. Secondly, when we later examine the effect of one oscillator on
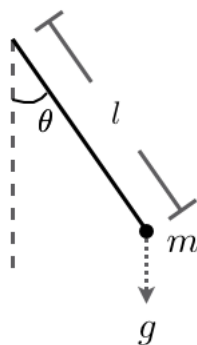
Figure 2.1: Simple pendulum where l is the length of the rod, m is mass, θ is the angle of displacement, and g is gravitational acceleration.
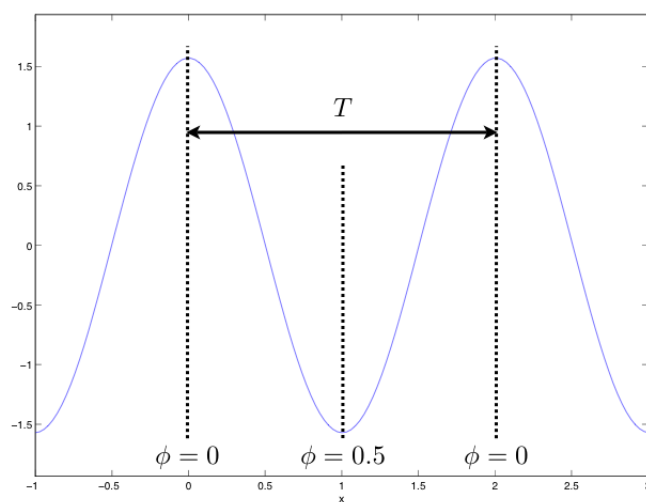
Figure 2.2: The particular solution $\theta(t) = \frac{\pi}{2}\cos\left(\sqrt{\frac{g}{l}}t\right)$ to (2.2) with $l = 1$ for initial conditions $\theta(0) = \frac{\pi}{2}$ and $\theta'(0) = 0$.

another, we are only concerned with phase as opposed to time. In this case, the phase is defined to be

$$\phi = \frac{t}{T} \mod 1, \tag{2.3}$$

where $T = 2\pi\sqrt{\frac{l}{g}}$ is the period of oscillation. Note that $0 \leq \phi < 1$. In this fairly simple situation, we have the following equation:

$$\frac{d\phi}{dt} = \omega, \tag{2.4}$$

where $\omega = \frac{1}{T} = \frac{\sqrt{g}}{2\pi\sqrt{l}}$ is the natural frequency of the oscillator.

We can now discuss collections of oscillators. A collection of n oscillators may be described by the variables $\phi_1, \ldots, \phi_n$, where $0 \leq \phi_i \leq 1$ is the phase of oscillator i. We still have the following simple equation

$$\frac{d\phi_i}{dt} = \omega_i, \tag{2.5}$$

where ω_i is the natural frequency of oscillator i. Such as system of uncoupled equations may represent a collection of independent pendula or neurons.

We can now consider *coupled* oscillators. Coupled oscillators respond to one another through a phase response function that describes the effect on an oscillator when another fires. Dutch physicist Christiaan Huygens invented and patented the pendulum clock in 1657. While recovering from an illness in his room several years later, Huygens began studying two clocks that were hanging next to one another on the wall. He realized that the swinging of the clocks' pendulums had somehow become synchronized. Huygens hypothesized that the synchronization was due to the clocks' proximity to one another. To test his hypothesis, Huygens moved the clocks to opposite sides of the room, where they began to lose synchrony. When the clocks were in close proximity, the motions of one pendulum could influence the other. However, when the clocks were far apart, they no longer had an effect on each other [12]. The two clocks are examples of weakly-coupled oscillators. The models and equations presented in this chapter are specifically designed for the behavior of weakly-coupled oscillators. The models assume that even after an oscillator's firing affects another, they will both settle back into their intrinsic firing pattern almost instaneously. The following equation describes a collection of oscillators in which all oscillators affect each other:

$$\frac{d\phi_i}{dt} = \omega_i + \varepsilon \sum_{j \neq i} F_{ij}(\phi_i, \phi_j), \tag{2.6}$$
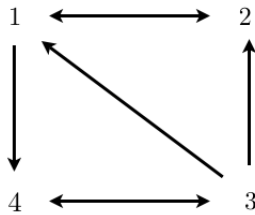
Figure 2.3: Example of a directed network topology
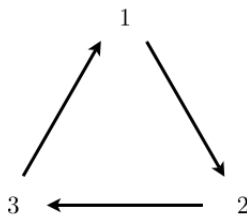
Figure 2.4: Network topology of three pulse-coupled oscillators

where ε is the coupling strength parameter, ϕ_i is the phase of oscillator i, ϕ_j is the phase of oscillator j, and F_{ij} is given by

$$F_{ij}(\phi_i, \phi_j) = S_i(\phi_i)H_j(\phi_j). \tag{2.7}$$

In this equation, we have separated F_{ij} into two parts, where each of the parts is only dependent on one of the oscillators. Here, $S_i(\phi_i)$ is the sensitivity function of oscillator i, and H_j is the signaling function of oscillator j.

The discussion of proximity also motivates the definition of a network. A network (graph) $G = (V, E)$ is an abstract object formed by a set V of nodes (vertices) and a set E of links (edges) that connect (join) pairs of nodes. If two nodes are connected by a link, they are adjacent. For example, in Figure 2.3, Node 1 is adjacent to Nodes 2 and 4, but it is not adjacent to Node 3. In the work that follows, we consider a directed network of three pulse-coupled oscillators (see Figure 2.4).

One model for coupled oscillators was originally constructed by Winfree in 1967 [13]. Winfree's model represents a large population of weakly-coupled oscillators with the following equation:

$$\frac{d\phi_i}{dt} = \omega_i + \varepsilon \sum_{j \neq i} A_{ji} F_{ij}(\phi_i, \phi_j), \tag{2.8}$$

where ϕ_i, ϕ_j, and F_{ij} are defined as above, and A_{ji} is the adjacency matrix for the network of pulse-coupled oscillators. In this equation, we do not necessarily assume that all oscillators affect one another. Winfree's model is a basis for many subsequent pulse-coupled oscillator systems, including the one discussed in this project.

In order to better model the types of biological systems described in Chapter 1, we now introduce *pulse-coupling*. For our purposes, pulse-coupling means that an oscillator fires and resets instantaneously, or practically instantaneously. This is tied to the signaling function, which is defined as follows:

$$H(\phi_j) = \delta(1 - \phi_j), \tag{2.9}$$

where δ is the Dirac delta function. The Dirac delta function is given by

$$\delta(x) = \begin{cases} +\infty, & x = 0 \\ 0, & x \neq 0. \end{cases} \tag{2.10}$$

Using Winfree's model and the Dirac delta function, we derive three equations used to model our network of three pulse-coupled oscillators. Let the *displacement function* be given by $\Delta_i(\phi_i, \varepsilon) = \varepsilon S_i(\phi_i)$. For $t < t_i^-$, where $\phi_i(t_i^-) = 1$, we have

$$\frac{d\phi_i}{dt} = \omega_i \text{ for } t < t_i^-, \text{ where } \phi_i(t_i^-) = 1, \tag{2.11}$$

and when $t = t_i^-$, we instantaneously update the oscillators phases as follows:

$$\begin{cases} \phi_i(t_i^+) = 0 \\ \phi_j \mapsto \phi_j(t_i) + \begin{cases} \Delta_j(\phi_j, \varepsilon) & \text{for } A_{ij} = 1 \\ 0 & \text{otherwise.} \end{cases} \end{cases} \tag{2.12}$$

For the non-general work that follows, we set $\varepsilon = 0.1$ and use the displacement function $\Delta(\phi) \equiv \Delta_i(\phi, \varepsilon) = \varepsilon \left[\sin\left(2\pi\phi + \frac{4\pi}{3}\right) - \sin\left(\frac{4\pi}{3}\right) \right]$ (see Figure 2.5).

We can think of our system, Equations (2.11) and (2.12), as a continuous time flow on $\mathbb{R}^3$. In order to analyze and better understand system dynamics, we discretize our system of three oscillators with respect to time and construct a mapping $f : \mathbb{R}^2 \to \mathbb{R}^2$ using a tool known as a Poincaré map. For $\underline{\phi} = \begin{bmatrix} \phi_1 \\ \phi_2 \end{bmatrix} \in \mathbb{R}^2, \underline{f}(\underline{\phi}) = \begin{bmatrix} f_1(\underline{\phi}) \\ f_2(\underline{\phi}) \end{bmatrix}$. To construct the map, we record the position of $\underline{\phi}$ right before the third

.1 (sin(2 π φ+(4 π/3))−sin(4 π/3))
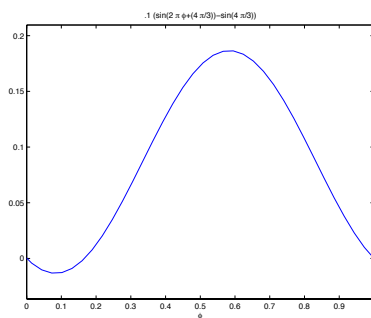
Figure 2.5: The specific phase-response curve used
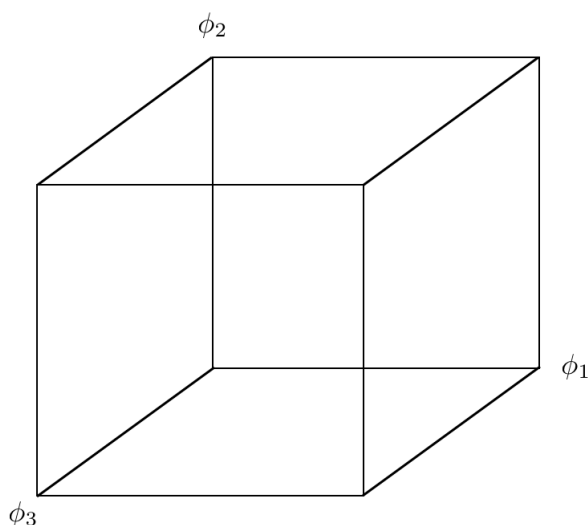
Figure 2.6: The unit cube

oscillator fires. We then record $\underline{\phi}$ right before the third oscillator fires again. This enables us to find an algebraic expression for the mapping. In other words, knowing ϕ_1 and ϕ_2 when the third oscillator fires, we can apply the valid mapping and find $\underline{f}(\underline{\phi})$, or the phases of oscillator 1 and 2, the next time oscillator 3 fires.

To think about the Poincaré map differently, we can think of the coordinates of the three oscillators moving around smoothly and continuously within the unit cube since $0 \leq \phi_i \leq 1$. When oscillator 3 is firing, $\phi_3 = 0 = 1$ because of the way the oscillators in this system fire and reset. Therefore, we are only concerned with the front and back square faces of the unit cube. See Figure 2.6. We want to find the algebraic expression that maps a point to one of these faces. In fact, the technique of the Poincaré map takes the initial point as $\phi_3 = 1 = 0$, so we are also concerned with an initial point on one of the front or back faces.This mapping does not depend on how the point travels through the unit cube. It only depends

Figure 2.7: The relevant portion of the decision-making tree if oscillator 2 fires next
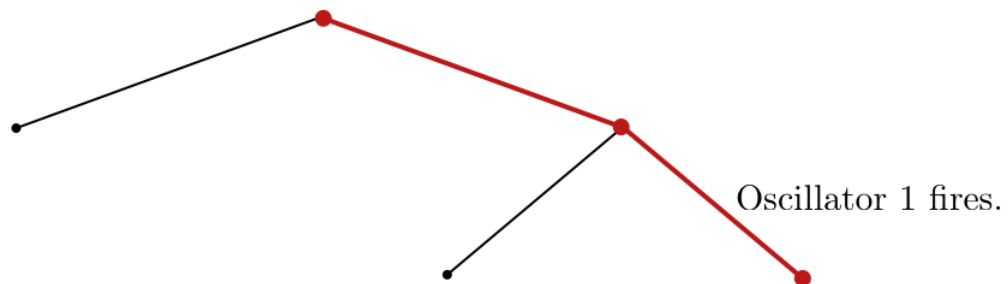
Figure 2.8: The relevant portion of the decision-making tree if oscillator 1 fires next

on the initial condition of the point. In his book *Sync* [11], Steven Strogatz likens the Poincaré map technique to taking two snapshots of the system, one when the third oscillator fires initially and another the next time it fires (see *Sync* for more details).

The mappings for our system depend on the initial conditions of the oscillators. The order in which the three oscillators fire depends on where the oscillators are in their phases compared to one another, and thus we can expect discontinuities in the Poincaré map of our system. To illustrate, using the network in Figure 2.4, we begin with the third oscillator firing. Therefore, the general coordinates of our system are $(\phi_1, \phi_2, 1)$. Then oscillator one responds and oscillator three resets, giving us the new coordinates $(\phi_1 + \Delta(\phi_1), \phi_2, 0)$. We must now decide whether oscillator 1 or 2 will fire next. Since the oscillators have the same frequency, this is determined by their relative ordering. Let us consider when oscillator 2 fires next, i.e. $d_r = \phi_2 - \phi_1 - \Delta(\phi_1) > 0$. See Appendix A for all of the branch point functions. This decision is illustrated by the tree in Figure 2.7. We are now only concerned with the right side of the tree. Suppose oscillator 1 fires next in the sequence of firing. Then we are concerned with $d_1 > 0$. Now we suppose that oscillator 3 fires again, ending this particular mapping case. Following all of the valid firing

Oscillator 3 fires.
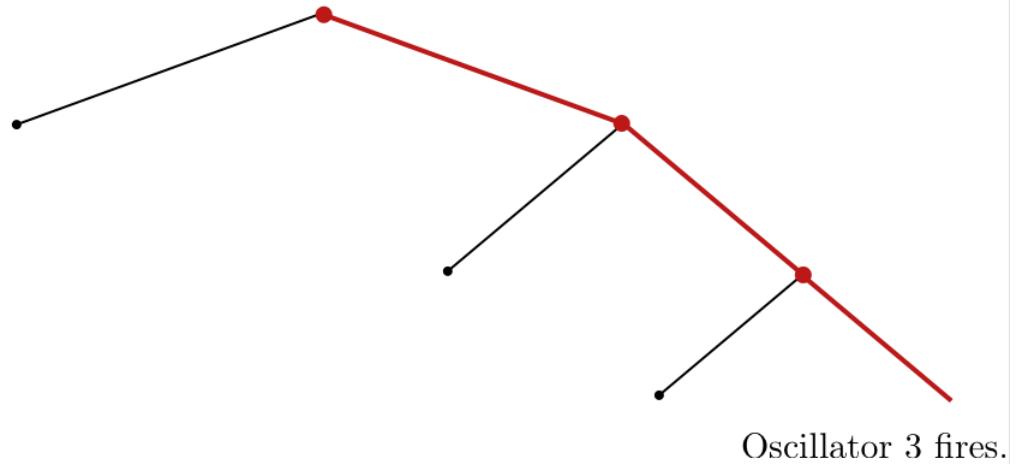
Figure 2.9: The entire path of oscillators that follow the sequence of firing represented by Case 6

sequences for this system results in the full decision-making tree.

Depending on where the oscillators were in their phases initially, the order of firing will be different. The branch points of the tree represent when two oscillators will fire at the same time. The leaves represent when oscillator 3 has fired and $\phi_3 = 1 = 0$ again. Our particular network topology and phase-response curve lead to six different cases or algebraic mappings that correspond to a certain set of initial conditions and introduce discontinuities into our system. If the order of firing is preserved for a set of initial conditions, then that portion of the Poincaré map is continuous. Discontinuities occur on the dividing curves, which is when two oscillators are firing at the same time. The six different mappings for the six different cases of the tree can be found in the appendix. The Poincaré map for Case 6 (see Figure 2.9) is given in equation (3.1). You can also see the unit square with the Poincaré map as the planes of intersection (see Figure 2.12).
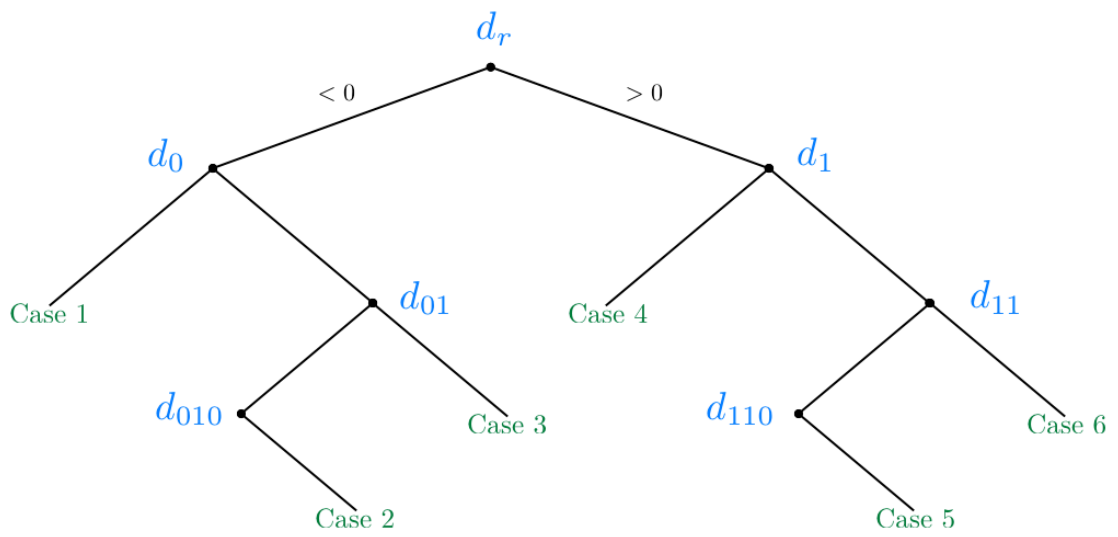
Figure 2.10: Full decision tree for the given ε and PRC
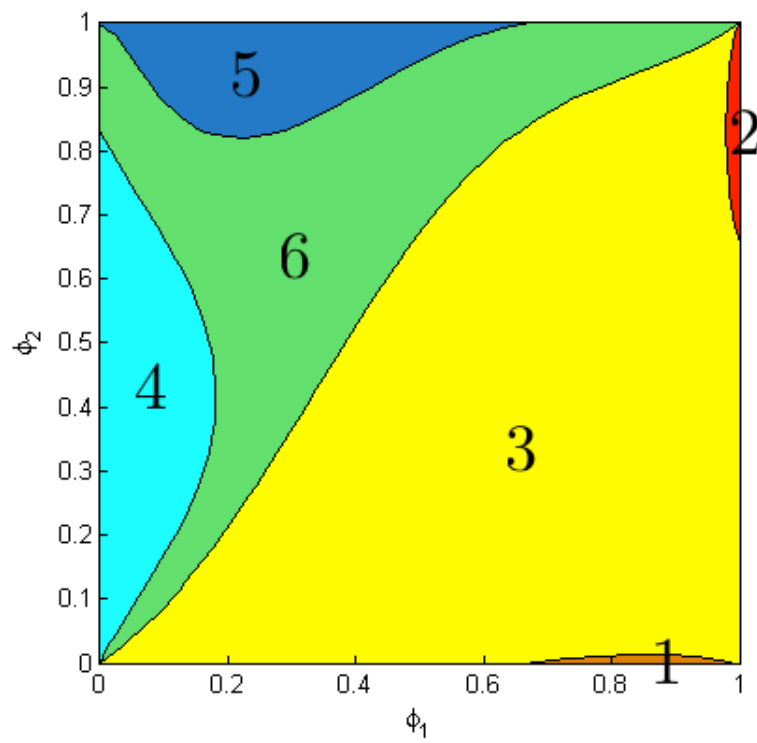
Figure 2.11: Graphical depiction of the domain for the Poincaré map f with regions of continuity and dividing lines where oscillators fire at the same time
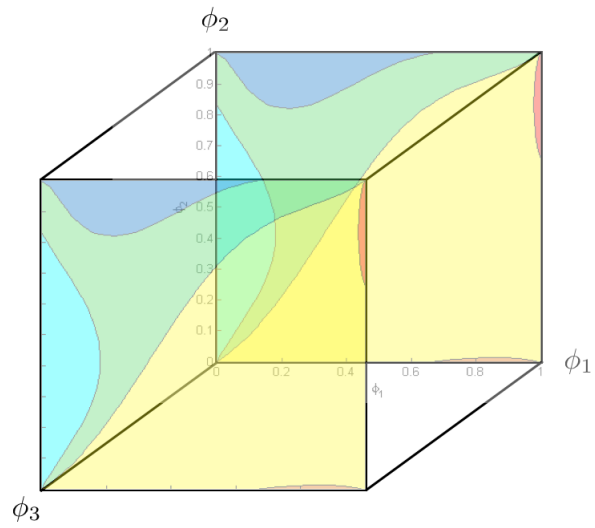
Figure 2.12: The Poincaré map overlaid with the Unit Square; the map represents the phases of intersection when oscillator 3 is firing.

Chapter 3

Analysis

Now that we have algebraic expressions for the Poincaré map on each of the six regions computed in Chapter 2, we can find and analyze *fixed points* for the map, where a fixed point is given by $\underline{f}(\underline{\phi}) = \underline{\phi}$. The algebraic expressions are sufficiently complicated that finding a closed-form, exact solution for the fixed points, either by hand or using computer software, is not feasible. However, using a numerical approximation found through MATLAB [6], we find that there is a fixed point in Region 6 near $(0.3095, 0.6905)$. The mappings for Region 6 are

$$
\begin{array}{rcl}
f_1(\phi_1, \phi_2) & = & \phi_1 + \Delta(\phi_1) - \Delta(1 - \phi_2), \\
f_2(\phi_1, \phi_2) & = & \phi_2 + \Delta(\phi_2 - \phi_1 - \Delta(\phi_1)) - \Delta(1 - \phi_2).
\end{array}
\tag{3.1}
$$

All other region mappings can be found in Appendix A. By setting these two equations equal to ϕ_1 and ϕ_2 respectively, we can solve for the fixed points of the system. We plotted these two lines using MATLAB and then searched for the intersection. This process is shown in Figure 3.1. The red lines represent $f_1(\phi_1, \phi_2) = \phi_1$, and the blue lines represent $f_2(\phi_1, \phi_2) = \phi_2$. There is only one intersection that occurs in the region for which the mapping is valid, meaning that there is only one valid fixed point in Region 6. The Jacobian matrix J, which is the linearization of the map, is defined by

$$
\left[
\begin{array}{cc}
\frac{\partial f_1}{\partial \phi_1} & \frac{\partial f_1}{\partial \phi_2} \\
\frac{\partial f_2}{\partial \phi_1} & \frac{\partial f_2}{\partial \phi_2}
\end{array}
\right].
$$

For the Jacobian of this system, see Appendix A. We use the eigenvalues of the Jacobian to determine the stability of fixed points. Since this project involves a discrete time system, if the magnitude of the leading eigenvalue (i.e. maximal in absolute value) is greater than 1, then the fixed point is unstable. If the leading value is less than 1, the fixed point is stable. All points in a sufficiently small neighborhood of a stable fixed point move closer to the fixed point in forward
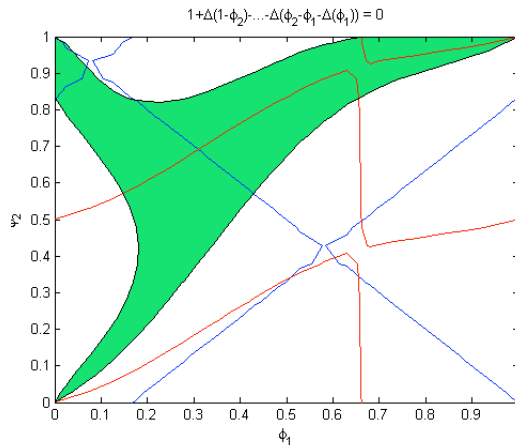
Figure 3.1: Fixed point found using intersection of fixed point equations

Point	Stability	Region
(0.3095, 0.6905)	Source	6
(0.5492, 0.2770)	Source	3
(0.6755, 0.3374)	Saddle	3
(0.4929, 0.1575)	Saddle	3
(0.4963, 0.3364)	Saddle	3

Table 3.1: A numerical approximation of all fixed points for our particular system along with their stability and region

time. In any neighborhood of an unstable fixed point, there exist some points that move farther away from the fixed point as time progresses. We find that for our particular fixed point,

$$J_{(0.3095, 0.6905)} = \begin{bmatrix} 1.6212 & 0.6212 \\ -1.007 & 2.2424 \end{bmatrix}.$$

The numerically computed eigenvalues for this matrix are $\lambda = 1.931 \pm 0.727i$. This corresponds to an unstable spiral source as depicted in Figure 3.2. We also numerically find four fixed points in Region 3. One fixed point is found near $(0.4963, 0.3364)$. The numerically computed eigenvalues for this point are $\lambda_1 = 1.6539$ and $\lambda_2 = 0.7347$. This corresponds to an unstable saddle. We can verify this behavior through simulation. Table 3.1 summarizes all fixed points and their stability.

We are interested in how system behavior changes as coupling strength ε varies. We create a bifurcation diagram, a general graphical representation of how dynamics change over a particular parameter, using PyCont, a sub-package of PyDSTool
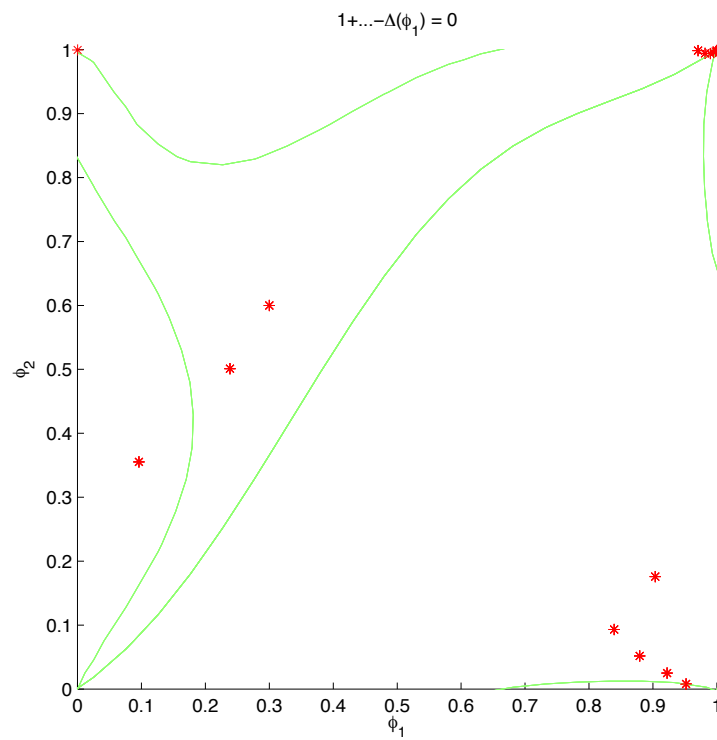
Figure 3.2: Simulation from the point $(0.3, 0.6)$ after 15 iterations; the point travels away from the fixed point (source) until it reaches the synchronous state located in the four corners of the unit square.
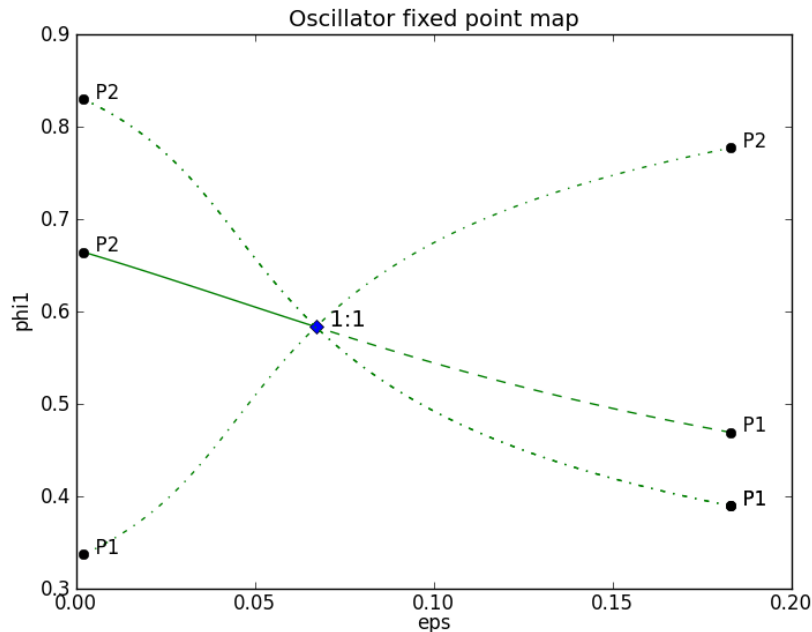
Figure 3.3: Bifurcation diagram for our system with ε on the horizontal axis and ϕ_1 on the vertical axis. Solid lines represent stable dynamics, dashed unstable, and dashed-dotted saddle points. One of the fixed points in Region 3 changes stability at a 1:1 resonant bifurcation point ($\varepsilon \approx 0.067$).

[2]. See Figure 3.3. Solid lines represent stable dynamics, dashed unstable, and dashed-dotted saddle. The bifurcation diagram appears to only have three lines, so visually the system only seems to have three fixed points in Region 3. However, Table 3.1 shows that there are four fixed points in this region. Two of the lines appear to be on top of one another at this resolution. This overlap is due to symmetry in the system; we are analyzing changes in ϕ_1 as ε changes, and two of the fixed points have sufficiently close ϕ_1 values to cause this overlap. We find a 1:1 resonant bifurcation (degenerate) near $\varepsilon = 0.067$. This type of bifurcation describes where the stability of a fixed point changes from a spiral sink to real eigenvalues to a spiral source. The bifurcation value of ε might also correspond to the stability of the synchronous state changing from stable to unstable (going in the direction of decreasing ε).
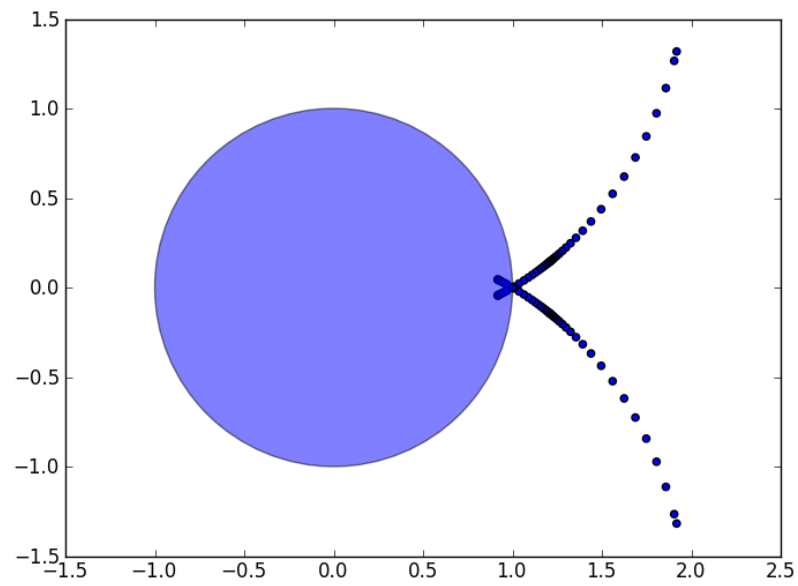
Figure 3.4: Complex plane showing scatter plot of the eigenvalues of the Jacobian for the source in Region 3 over varying epsilon (corresponding to middle curve in Figure 3.3), with blue circle illustrating the unit circle.

Chapter 4

Computational Approach and Algorithms

We will now introduce a computational tool called the *Conley index* from algebraic topology which will allow us to make rigorous measurements of fixed points and connecting orbits. We will build an example using sample results.

Let $f : \mathbb{R}^n \rightarrow \mathbb{R}^n$ be a continuous map. A *trajectory through* $x \in \mathbb{R}^n$ is a sequence

$$\gamma_x := (\ldots, x_{-1}, x_0, x_1, \ldots) \tag{4.1}$$

such that $x_0 = x$ and $x_{n+1} = f(x_n)$ for all $n \in \mathbb{Z}$. We now define the *invariant set relative to $N \subset \mathbb{R}^n$* as

$$\text{Inv}(N, f) := \{x \in N | \text{ there exists a trajectory } \gamma_x \text{ with } \gamma_x \subset N\} \tag{4.2}$$

Definition 4.0.1. *A compact set $N \subset \mathbb{R}^n$ is an* isolating neighborhood *if*

$$\text{Inv}(N, f) \subset \text{int}(N) \tag{4.3}$$

where $\text{int}(N)$ *denotes the interior of N. S is an* isolated invariant set *if $S = \text{Inv}(N, f)$ for some isolating neighborhood N.*

Definition 4.0.2. *Let $P = (P_1, P_0)$ be a pair of compact sets with $P_0 \subset P_1 \subset X$. The map induced on the pointed quotient space $(P_1/P_0, [P_0])$ is*

$$f_P(x) := \begin{cases} f(x) & \text{if } x, f(x) \in P_1 \setminus P_0 \\ [P_0] & \text{otherwise} \end{cases} \tag{4.4}$$

Definition 4.0.3. *([10]) The pair of compact sets $P = (P_1, P_0)$ with $P_0 \subset P_1 \subset X$*

is an index pair *for f provided that*

1. *the induced map, f_P, is continuous,*

2. *$\overline{P_1 \setminus P_0}$, the closure of $P_1 \setminus P_0$, is an isolating neighborhood.*

In this case, we say that P is an index pair for the isolated invariant set $S = \text{Inv}(\overline{P_1 \setminus P_0}, f)$. In this project, sometimes we compute P where the map is discontinuous. In this case, we call it a pair. It is not an index pair since Conley index theory breaks down in regions of discontinuity.

Definition 4.0.4. *Two group homomorphisms, $\phi : G \to G$ and $\psi : G' \to G'$ on abelian groups G and G' are* shift equivalent *if there exist group homomorphisms $r : G \to G'$ and $s : G' \to G$ and a constant $m \in \mathbb{N}$ (referred to as the 'lag') such that*

$$r \circ \phi = \psi \circ r, \quad s \circ \psi = \phi \circ s, \quad r \circ s = \psi^m, \quad and \quad s \circ r = \phi^m.$$

The shift equivalence class of ϕ, *denoted $[\phi]_s$, is the set of all homomorphisms ψ such that ψ is shift equivalent to ϕ.*

Definition 4.0.5. *Let $P = (P_1, P_0)$ be an index pair for the isolated invariant set $S = \text{Inv}(\overline{P_1 \setminus P_0}, f)$ and let $f_{P*} : H_*(P_1, P_0) \to H_*(P_1, P_0)$ be the map induced on the relative homology groups $H_*(P_1, P_0)$ from the map f_P. The* Conley index of S *is the shift equivalence class of f_{P*}*

$$\text{Con}(S, f) := [f_{P*}]_s. \tag{4.5}$$

Theorem 4.0.6. *If $\text{Con}(S, f) \neq [0]_s$, then $S \neq \emptyset$.*

Definition 4.0.7. *Let S be an isolated invariant set. The* Lefschetz number of S *is defined as*

$$L(S, f) := \sum_k (-1)^k \, \text{tr}(f_{Pk}) \tag{4.6}$$

where $P = (P_1, P_0)$ is an index pair for S.

The Lefschetz number is essential to the following theorem and its corollary. For the index pair in Figure 4.1, homcubes (see Appendix) shows that the resulting map on homology is the identity, and thus, corresponds to the identity matrix. For our example, k = 2. The H_2 group is equal to $\mathbb{Z}$, meaning that it is generated by one copy of $\mathbb{Z}$. Therefore, $f_{Pk} = [1]$. Thus, $L(S, f) = 1$.
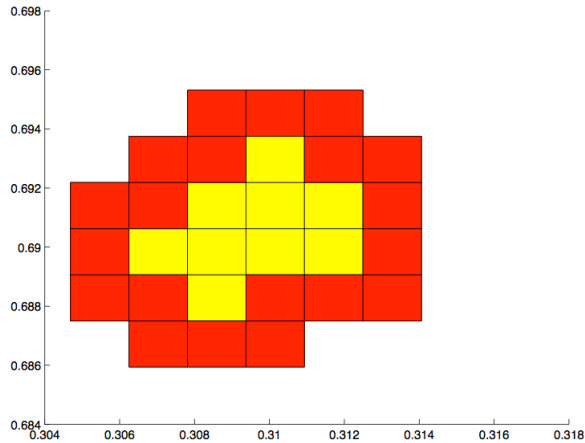
Figure 4.1: An index pair; the light region represents the isolating neighborhood, and the dark region represents the exit set. Together they form the entire index pair.

Theorem 4.0.8. *Let S be an isolated invariant set. If*

$$L(S, f) \neq 0, \tag{4.7}$$

then S contains a fixed point.

For a proof, see [14]. Thus, the index pair in Figure 5.3 contains a fixed point.

The Conley index is naturally suited for a computational approach. More specifically, using an *outer enclosure* for f on a uniform grid, we may use the algorithms given in Appendix B to construct isolating neighborhoods and index pairs for f.

We begin by using the subdivision procedure implemented in the software package *GAIO* [5] to create a grid $\mathcal{G}$ on a compact (rectangular) region in X. In practice, the region chosen for representation is usually determined either experimentally through non-rigorous numerical simulations or analytically given a special structure or symmetry for the system (e.g. a compact attracting region). We partition a specified rectangular set $W = \prod_{k=1}^{n}[x_k^-, x_k^+] \subset \mathbb{R}^n$ into a *cubical grid*

$$\mathcal{G}^{(d)} := \left\{ \prod_{k=1}^{n} \left[x_k^- + \frac{i_k r_k}{2^d}, x_k^- + \frac{(i_k+1)r_k}{2^d} \right] \,\middle|\, i_k \in \left\{0, \ldots, 2^d - 1\right\} \right\}$$

where $r_k = x_k^+ - x_k^-$ is the radius of W in the kth coordinate and the depth d is a nonnegative integer. We call an element of the grid, $B = \prod_{k=1}^{n} \left[x_k^- + \frac{i_k r_k}{2^d}, x_k^- + \frac{(i_k+1)r_k}{2^d} \right]$, a *box*. For a collection of boxes, $G \subset \mathcal{G} = \mathcal{G}^{(d)}$, define the *topological realization* of G as $|G| := \cup_{B \in G} B \subset \mathbb{R}^n$.

The index pair shown in this section was constructed on a grid on the unit square at depth $d = 16$.

Definition 4.0.9. *Given a continuous map $f : \mathbb{R}^n \to \mathbb{R}^n$, a map $\mathcal{F} : \mathcal{G} \rightrightarrows \mathcal{G}$ from $\mathcal{G}$ to its power set is a* (combinatorial) outer enclosure *if for each $G \in \mathcal{G}$*

$$\{G'|f(|G|) \cap |G'| \neq \emptyset\} \subset \mathcal{F}(G)$$

and $|\mathcal{F}(G)|$ is acyclic (i.e. has the homology of a point).

Algorithmically, it may be better to think of $\mathcal{F}$ as a directed graph where the ith vertex corresponds to the ith grid element G_i and there exists a directed edge from vertex i to vertex j if $G_j \in \mathcal{F}(G_i)$. Note that if $f(x) = x$, then there must be a self loop in $\mathcal{F}$ (a directed edge from i to i for G_i containing x). More generally, dynamics for f forces structure in $\mathcal{F}$. For our purposes, one really nice property of the outer enclosure is that there exist algorithms for growing isolating neighborhoods and index pairs. These algorithms, which were used to compute the isolating neighborhoods shown here, can be found in [4]. Given an index pair in the outer enclosure, we use the software package CHomP [1] to compute the associated Conley Index. These tools will be used in Chapter 5 to construct a picture of the global dynamics for our model.

Chapter 5

Results

In what follows, we use the software package GAIO (Global Analysis of Invariant Objects) [5] with a MATLAB [6] interface to create a uniform grid on the unit square. We construct an outer enclosure by first testing which region a given grid element is in. Note that a grid element may possibly intersect multiple regions. For each region that a grid element intersects, we compute the image of that grid element under the map constructed using the decision tree and then set the outer enclosure to the union of these images. All computations are performed using outward rounding interval arithmetic through INTLAB [3] to account for truncation error. Homology information is computed using CHomP [1].

We now use the tools outlined in Chapters 2 and 4 to compute information about the global dynamics for Equations (2.11) and (2.12) with $\varepsilon = 0.1$. We cannot vary ε widely because as ε varies, our Poincaré map changes. These computations are for our particular network topology, Poincaré map, and phase response function. We begin with a discussion of resolution. Depending on the depth we choose for our grid in GAIO, we get a very different understanding of our system. A higher resolution results in more boxes in our grid. Therefore, higher resolutions lead to a better and better outer enclosure. A higher resolution allows us to isolate fixed points, meaning that the index pairs isolate dynamics from one fixed point as opposed to a region of several locationally close fixed points. However, higher resolution tree structures take longer to store and perform computations, especially the computation of the transition matrix. Figure 5.1 shows the difference between a course grid resolution and a finer grid resolution.

We note that the trajectories of many initial conditions seem to limit in forward time to the synchronous state $(\phi_1, \phi_2) \in \{0, 1\} \times \{0, 1\}$ when all three of the oscillators synchronize and begin firing in unison. This collection of initial conditions is called the *basin of attraction* for the synchronous state. Using a trapping region consisting of the four synchronous corner points $(0, 0), (0, 1), (1, 0), (1, 1)$, we iden-
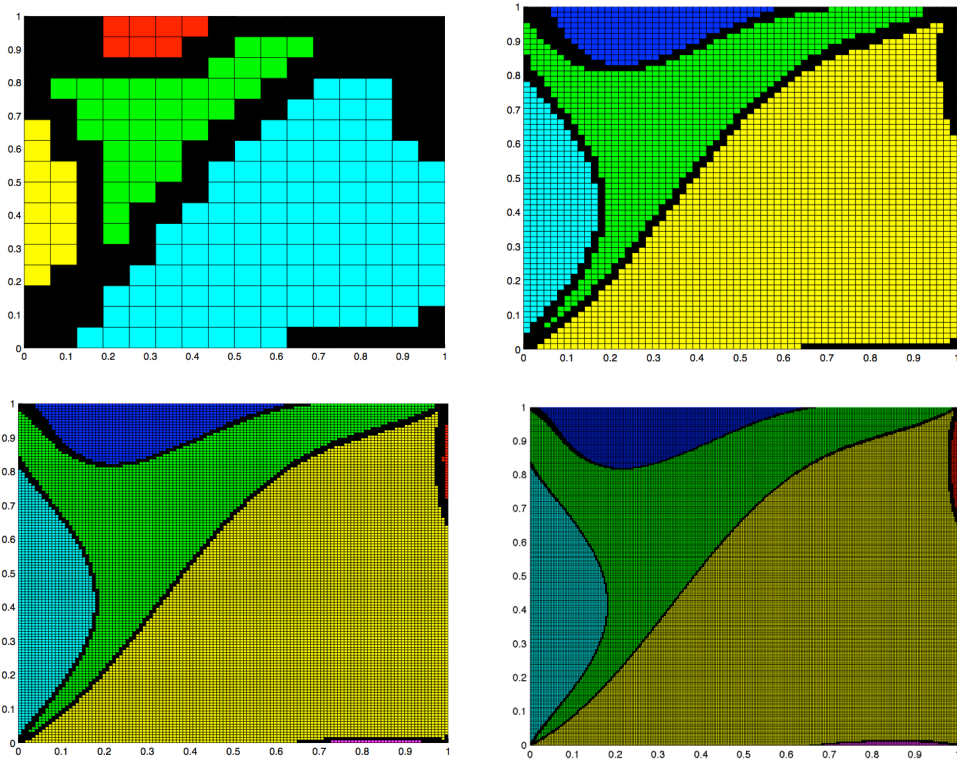
Figure 5.1: Poincaré map constructed from GAIO boxes at grid depths of 8, 12, 14, and 16 respectively.

tify all grid elements whose forward image eventually enters the (stable) isolating neighborhood for the synchronous state. This trapping region is not technically an outer enclosure because the synchronous region contains lines of discontinuity, but it functions in a similar manner. This computer collection is in the basin of attraction for the (small) isolating neighborhood of the synchronous state. (This isolating neighborhood is depicted in red in Figure 5.2.) Since the exit set for this neighborhood is empty, trajectories that enter this neighborhood remain in the neighborhood for all forward time. We strongly suspect that these trajectories limit to the synchronous state, but more work would be required to verify this. The region shown in blue in Figure 5.2 is computed using MATLAB code written by Georgia Pfeiffer in [8], and shows initial conditions in the basin of attraction for the isolating neighborhood of the synchronous state. Note that if a trajectory enters the trapping region, dynamics are simple and don't need to be studied any further. Because everything in the basin is sure to travel to the synchronous state in forward time, you can throw out all of the basin boxes when searching for asynchronous behavior. This means far fewer boxes in the tree structure, so we can refine the tree
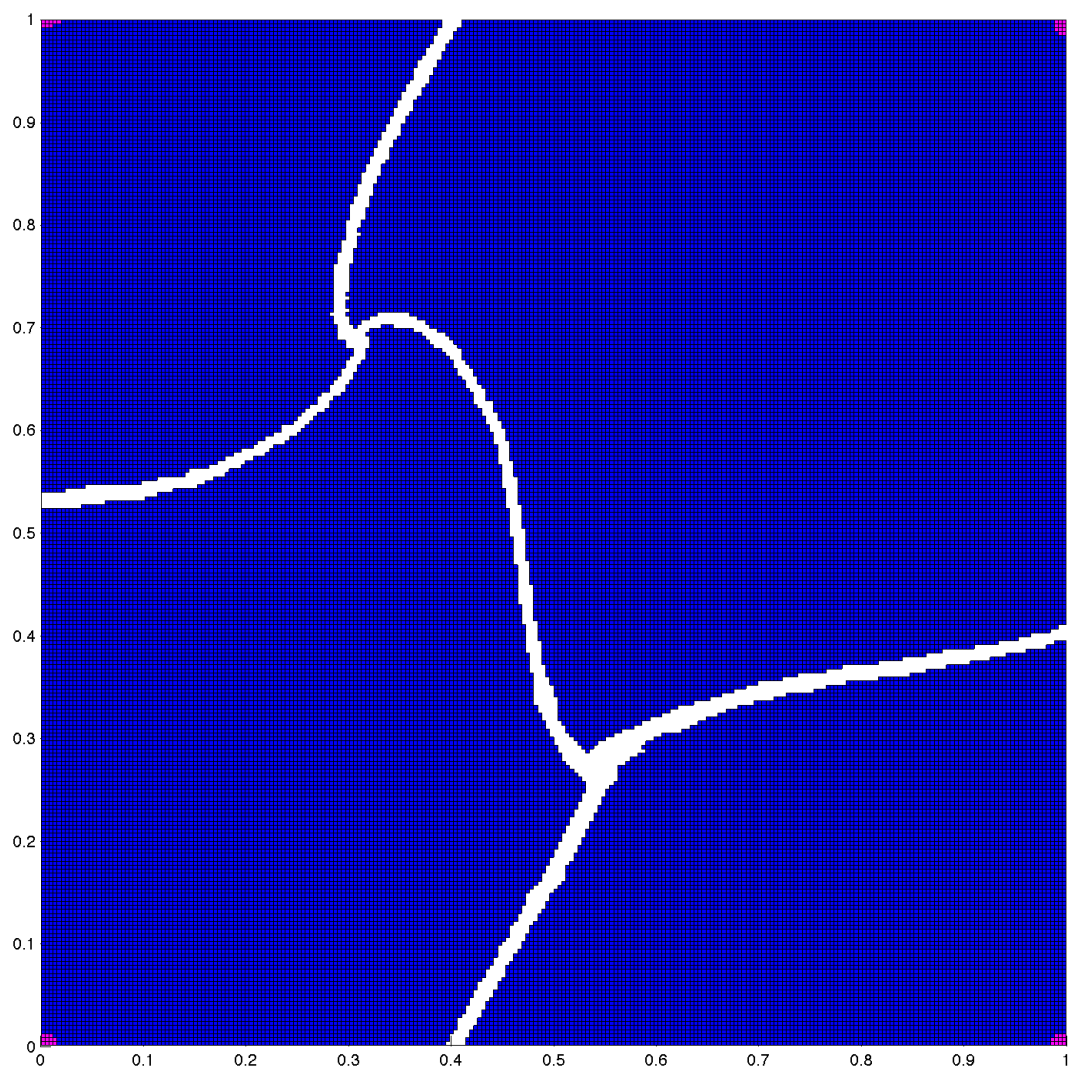
Figure 5.2: Basin of Attraction at Depth 16: The basin is shown in blue, and the trapping region is depicted in magenta.

Figure 5.3: Pair 6A, a source-type index pair containing a fixed point in Region 6.
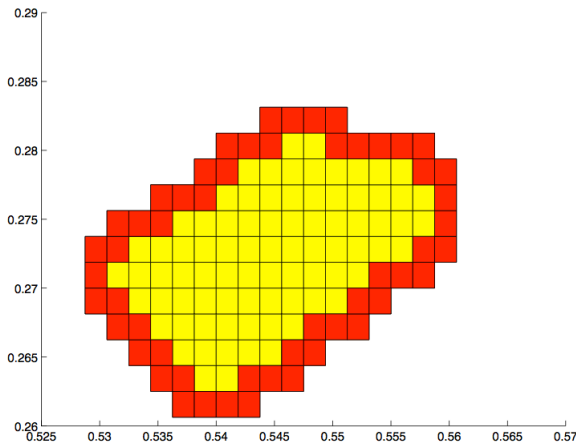
Figure 5.4: Pair 3A, a source-type index pair containing a fixed point in Region 3.

to a higher resolution much more quickly. To search for global system dynamics, we used a grid at depth 14. We then computed the basin of attraction, removed all the basin boxes, and refined to a depth of 16. This depth allows us to isolate fixed point dynamics.

Using the Lefschetz fixed-point theorem and homcubes output, we can rigorously prove that these five index pairs contain fixed points. The exit sets, or regions in red, suggest the behavior of the fixed points. Two-dimensional exit sets suggest unstable source behavior, while one-dimensional exit sets suggest unstable saddle behavior. Zero-dimensional exit sets suggest stable sink behavior. These index pairs suggest fixed point behavior that matches linearization techniques used in MATLAB. Individually, these index pairs reveal local dynamics. But through these
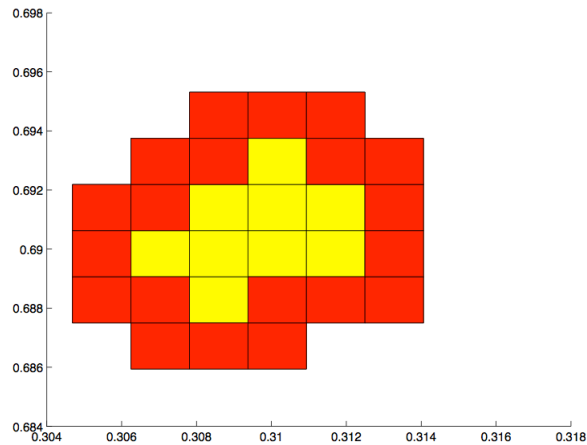
Figure 5.5: Pair 3B, a saddle-type index pair containing a fixed point in Region 3.

Figure 5.6: Pair 3C, a saddle-type index pair containing a fixed point in Region 3.

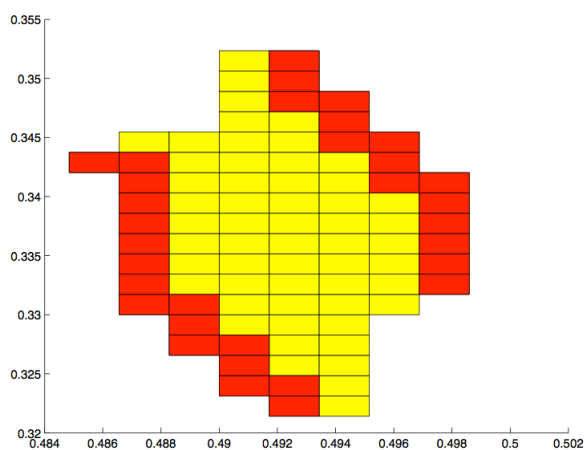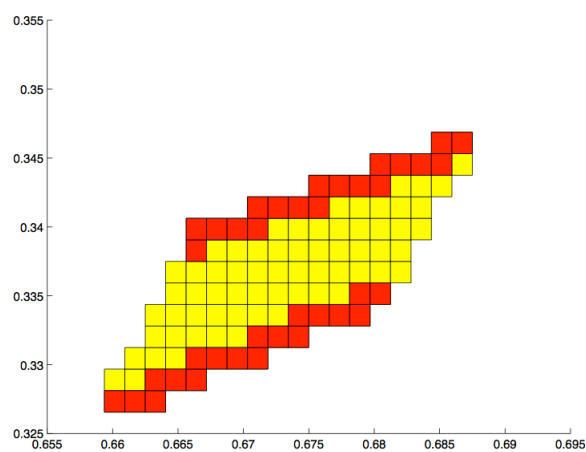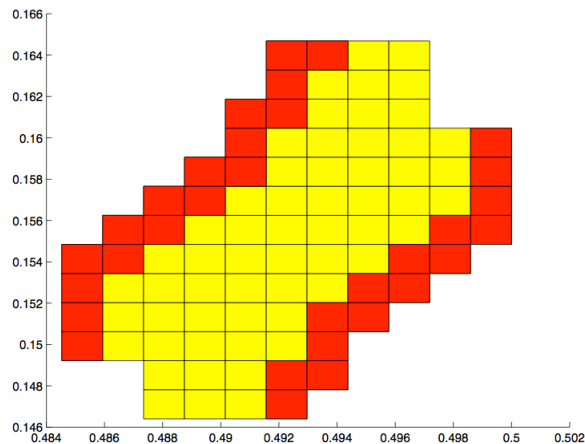Figure 5.7: Pair 3D, a saddle-type index pair containing a fixed point in Region 3.

index pairs, we are getting closer to understanding global dynamics.

For all of the continuous regions, we can prove that these index pairs contain isolating neighborhoods. In what follows, we will need to define a *strongly connected component*. A strongly connected component is a maximal strongly connected subgraph, where a subgraph is strongly connected when any two vertices have a directed path between them in both directions. First, we confirm that there are strongly connected components where both of the fixed points are located and nowhere else. Then we show that there is a path, or multiple paths, in one direction of the connecting orbit but not in the other direction. Once this has been verified, we can use Conley index theory to support what we have found graphically. If a connecting orbit exists, the homology groups for the connecting orbit should not equal the sum of the homology groups of the fixed points contained in the connecting orbit. Thus, we can rigorously prove that these index pairs contain a connecting orbit.

We have now analyzed dynamics across the phase space. See Table 5.1 for a summary of the computed dynamics. Fixed points are named by the region they are located in followed by a letter. Connecting orbits are named by the fixed points they connect. Pair S is the pair used to study the synchronous state.

Our analysis of the synchronous state is a special case since Pair S is not an index pair. The Poincaré map is discontinuous at the synchronous state, forcing the first condition in the definition of an index pair to be violated for any pair P containing the synchronous state. (See Definition 4.0.3). Since we cannot compute an index pair, we are not able to use Conley index theory to analyze this fixed point. However, using the `grow_isolated` algorithm followed by the `build_IP` algorithm, we obtain a pair $P = (P_1, P_0)$ that consists of P_1, a small neighborhood of the
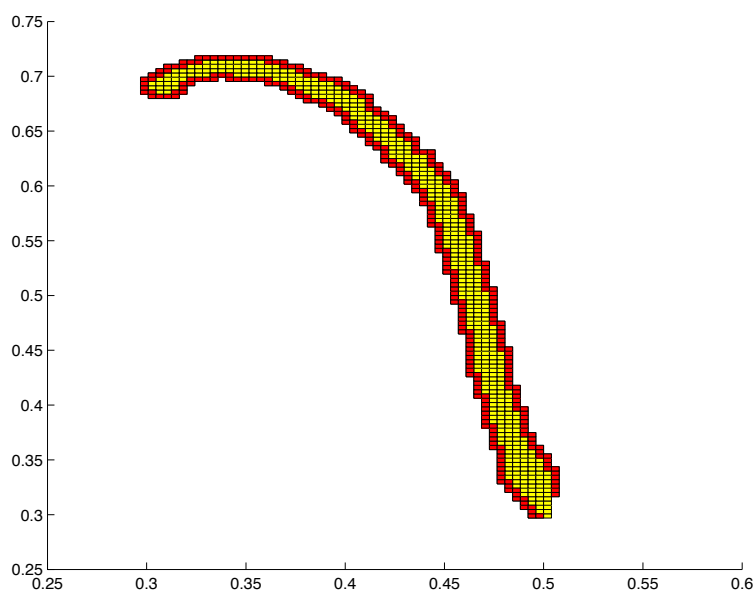
Figure 5.8: Pair 6A-3B, a connecting orbit between the source-type region depicted in Figure 5.3 and saddle-type region depicted in Figure 5.5.
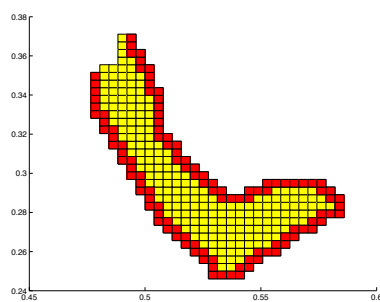
Figure 5.9: Pair 3A-3B, index pair for a connecting orbit.
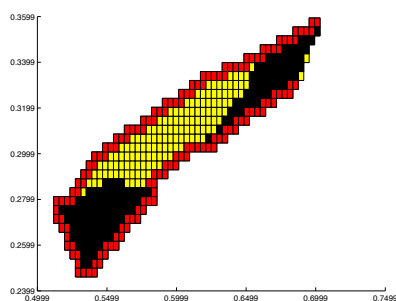
Figure 5.10: Pair 3A-3C, index pair for a connecting orbit.
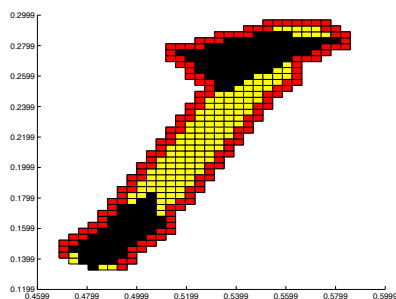
Figure 5.11: Pair 3A-3D, index pair for a connecting orbit.
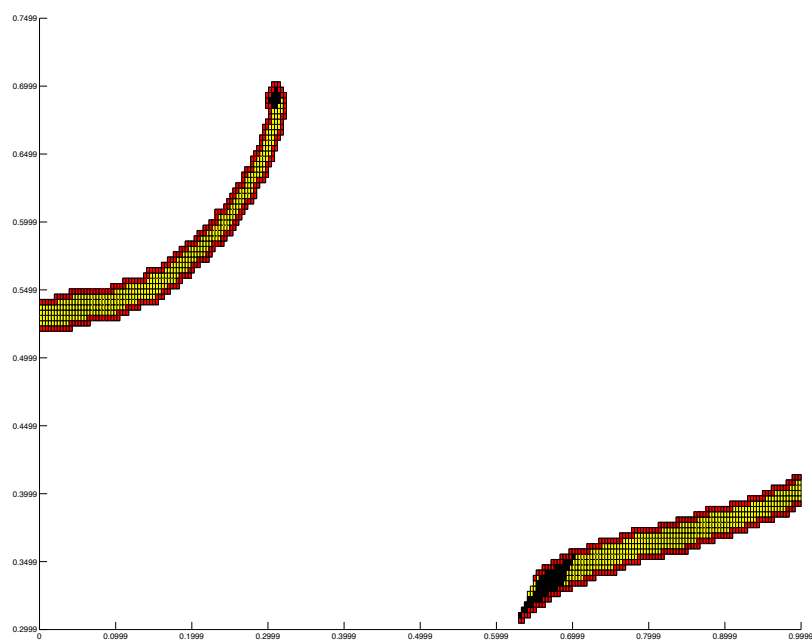
Figure 5.12: Pair 6A-3C, pair for a connecting orbit strongly suggested by numerical computation.
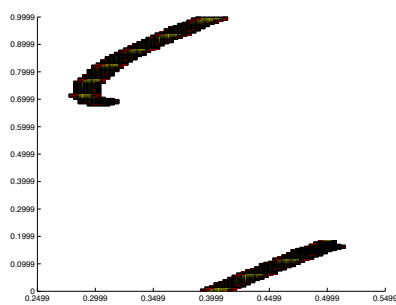
Figure 5.13: Pair 6A-3D, pair for a connecting orbit strongly suggested by numerical computation.
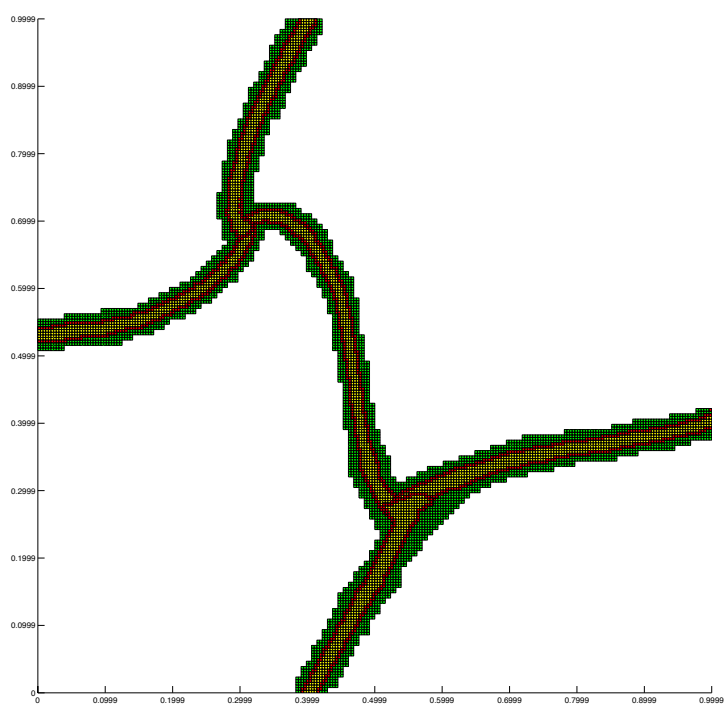
Figure 5.14: All connecting orbits for this system
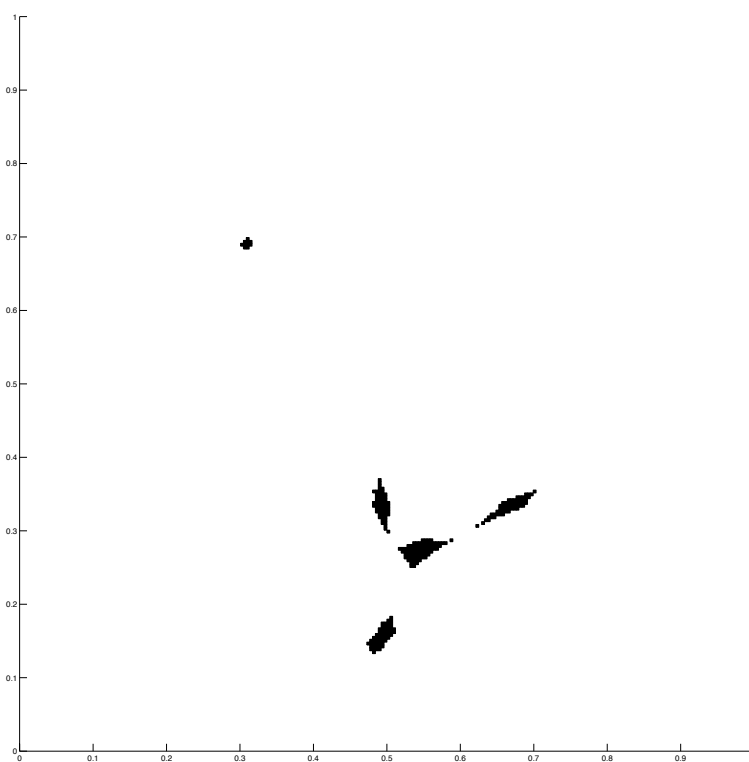
Figure 5.15: All strongly connected components for this system

synchronous state and the empty set for P_0 (the exit set position). The set P_1 acts as a trapping region. More specifically, mapping a one-box neighborhood of P_1 forward using the outer enclosure of the Poincaré map gives an image that is inside P_1. Therefore any initial condition in P_1 has a trajectory that remains in the set for all time. We strongly suspect that all such trajectories limit to the synchronous state, but cannot use our current techniques to prove it. The next listed sample result in the table is that of a basin of attraction for P_1. This collection of boxes contains points whose trajectories enter P_1 after a finite number of steps. Again, we strongly suspect that the trajectories of points in this region limit to the synchronous state, but we can only conclude that they enter the small trapping region around the synchronous state using our current approach.

Pair	Homology Groups, $H_k(P_1, P_0)$	Map on Homology, f_{Pk}	Interpretation
S	$\begin{cases} \mathbb{Z} & \text{for } k = 0 \\ 0 & \text{otherwise} \end{cases}$	$\begin{cases} [1] & \text{for } k = 0 \\ 0 & \text{otherwise} \end{cases}$	Trapping region containing the synchronous state
B	$\begin{cases} \mathbb{Z} & \text{for } k = 0 \\ 0 & \text{otherwise} \end{cases}$	$\begin{cases} [1] & \text{for } k = 0 \\ 0 & \text{otherwise} \end{cases}$	Basin of attraction for Pair S
6A	$\begin{cases} \mathbb{Z} & \text{for } k = 2 \\ 0 & \text{otherwise} \end{cases}$	$\begin{cases} [1] & \text{for } k = 2 \\ 0 & \text{otherwise} \end{cases}$	Source-type fixed point verified by Lefschetz number computation
3A	$\begin{cases} \mathbb{Z} & \text{for } k = 2 \\ 0 & \text{otherwise} \end{cases}$	$\begin{cases} [1] & \text{for } k = 2 \\ 0 & \text{otherwise} \end{cases}$	Source-type fixed point verified by Lefschetz number computation
3B	$\begin{cases} \mathbb{Z} & \text{for } k = 1 \\ 0 & \text{otherwise} \end{cases}$	$\begin{cases} [1] & \text{for } k = 1 \\ 0 & \text{otherwise} \end{cases}$	Saddle-type fixed point verified by Lefschetz number computation
3C	$\begin{cases} \mathbb{Z} & \text{for } k = 1 \\ 0 & \text{otherwise} \end{cases}$	$\begin{cases} [1] & \text{for } k = 1 \\ 0 & \text{otherwise} \end{cases}$	Saddle-type fixed point verified by Lefschetz number computation
3D	$\begin{cases} \mathbb{Z} & \text{for } k = 1 \\ 0 & \text{otherwise} \end{cases}$	$\begin{cases} [1] & \text{for } k = 1 \\ 0 & \text{otherwise} \end{cases}$	Saddle-type fixed point verified by Lefschetz number computation
3A-3B	0 for all k	0 for all k	Connecting orbit verified by Conley index theory
3A-3C	0 for all k	0 for all k	Connecting orbit verified by Conley index theory
3A-3D	0 for all k	0 for all k	Connecting orbit verified by Conley index theory
6A-3B	0 for all k	0 for all k	Connecting orbit verified by Conley index theory
6A-3C	0 for all k	0 for all k	Connecting orbit suggested by numerical computations
6A-3D	0 for all k	0 for all k	Connecting orbit suggested by numerical computations

Table 5.1: This table summarizes the computed dynamics of our system.

Chapter 6

Conclusion

We developed the algorithms necessary to find and analyze global dynamics for a system of pulse-coupled oscillators. Despite the limitations of common analytical techniques, we have succeeded in rigorously computing the basin of attraction for our system and locating gradient-like behavior (fixed points and connecting orbits) through the use of a decision tree, Poincaré map, and topological tools.

In the future, we hope to apply the algorithms used in this research to a wide range of general dynamic systems. For example, we hope to analyze global dynamics over different network topologies, phase response functions, and parameters using database software, which is a rigorous discovery of dynamical behavior in parameter space. In this project, we assumed that all oscillators behave in the same way. For example, they all have the same coupling strength and same frequency. But it is possible to find drastically different behavior if we allow these parameters to vary in a heterogeneous way. These efforts will be greatly aided by automating the building of the decision tree and Poincaré map.

Bibliography

[1] Computational Homology Project (CHomP). (http://www.math.gatech.edu/∽chomp/).

[2] RH Clewley, WE Sherwood, MD LaMar, and JM Guckenheimer. PyD-STool, a software environment for dynamical systems modeling, 2007. http://pydstool.sourceforge.net.

[3] Tibor Csendes, editor. *INTLAB - INTerval LABoratory*, Dordrecht, 1999. Springer. Proceedings of the International Symposium on Scientific Computing, Computer Arithmetic and Validated Numerics. Selected papers from the symposium (SCAN-98) held in Budapest, September 22–25, 1998, Reprinted in *Developments in reliable computing* [213–357, Kluwer Acad. Publ., Dordrecht, 1999], Reliab. Comput. **5** (1999), no. 3.

[4] Sarah Day, Rafael Frongillo, and Rodrigo Treviño. Algorithms for rigorous entropy bounds and symbolic dynamics. *SIAM J. Appl. Dyn. Syst.*, 7(4):1477–1506, 2008.

[5] Michael Dellnitz, Gary Froyland, and Oliver Junge. The algorithms behind GAIO-set oriented numerical methods for dynamical systems. In *Ergodic theory, analysis, and efficient simulation of dynamical systems*, pages 145–174, 805–807. Springer, Berlin, 2001.

[6] MATLAB. *version 7.13.0 (R2011b)*. The MathWorks Inc., Natick, Massachusetts, 2011.

[7] Renato Mirollo and Steven Strogatz. Synchronization of pulse-coupled biological oscillators. *SIAM J. Appl. Math.*, 50(6):1645–1662, 1990.

[8] Georgia Waite Pfeiffer. Basins of attraction in stage structured populations. Honor's thesis, College of William and Mary, 2011.

[9] Juan G Restrepo, Edward Ott, and Brian R Hunt. Onset of synchronization in large networks of coupled oscillators. *Phys. Rev. E*, 71(3 Pt 2A):036151, Mar 2005.

[10] Joel W. Robbin and Dietmar Salamon. Dynamical systems, shape theory and the Conley index. *Ergodic Theory Dynam. Systems*, 8*(Charles Conley Memorial Issue):375–393, 1988.

[11] Steven Strogatz. *Sync: The Emerging Science of Spontaneous Order*. Hyperion, New York, New York, 2003.

[12] Steven Strogatz and Ian Stewart. Coupled oscillators and biological synchronization. *Scientific American*, 269(6):68–74, Dec 1993.

[13] Steven H Strogatz. From kuramoto to crawford: exploring the onset of synchronization in populations of coupled oscillators. *Physica D: Nonlinear Phenomena*, 143(1-4):1–20, Sep 2000.

[14] Andrzej Szymczak. The Conley index and symbolic dynamics. *Topology*, 35(2):287–299, 1996.

[15] Marc Timme, Fred Wolf, and Theo Geisel. Prevalence of unstable attractors in networks of pulse-coupled oscillators. *Phys. Rev. Lett.*, 89(15):154105, Sep 2002.

Appendix A

Further Analysis and Sample Results

A.1 Dividing Line Equations

Subscripts correspond to a certain branch point, which give the dividing curve expression. See Figure 2.10.

$$d_r = \phi_2 - \phi_1 - \Delta(\phi_1) = 0$$

$$d_0 = \phi_2 + \Delta(\phi_2 + 1 - \phi_1 - \Delta(\phi_1)) = 0$$

$$d_1 = \phi_1 + \Delta(\phi_1) - \Delta(1 - \phi_2) = 0$$

$$d_{01} = 1 + \Delta(1 - \phi_2 - \Delta(\phi_2 + 1 - \phi_1 - \Delta(\phi_1))) - \phi_1 - \Delta(\phi_1) = 0$$

$$d_{11} = 1 + \Delta(1 - \phi - 2) - \phi_2 - \Delta(\phi_2 - \phi_1 - \Delta(\phi_1)) = 0$$

$$d_{010} = 1 - \phi_2 - \Delta(\phi_2 - \Delta(\phi_2 + 1 - \phi_1 - \Delta(\phi_1))) - \Delta(1 - \phi_1 + \phi_2 - \Delta(\phi_1) \\ + \Delta(\phi_2 + 1 - \phi_1 - \Delta(\phi_1))) = 0$$

$$d_{110} = 1 + \Delta(1 - \phi_2) - \Delta(\phi_2 - \phi_1 - \Delta(\phi_1)) + \Delta(2 - \phi_2 + \Delta(1 - \phi_2) \\ - \Delta(\phi_2 - \phi_1 - \Delta(\phi_1))) - \phi_1 = 0$$

A.2 Region Mappings

Region 1:

$$\bar{\phi}_1 = \phi_1 + \Delta(\phi_1)$$
$$\bar{\phi}_2 = \phi_2 + 1 + \Delta(\phi_2 + 1 - \phi_1 - \Delta(\phi_1))$$

Region 2:

$$\bar{\phi}_1 = \phi_1 + \Delta(\phi_1) - 1 - \Delta(1 - \phi_2 - \Delta(\phi_2 + 1 - \phi_1 - \Delta(\phi_1)))$$
$$\bar{\phi}_2 = \phi_2 + \Delta(\phi_2 + 1 - \phi_1 - \Delta(\phi_1))$$
$$+ \Delta(1 - \phi_1 + \phi_2 - \Delta(\phi_1) + \Delta(\phi_2 + 1 - \phi_1 - \Delta(\phi_1)))$$
$$- \Delta(1 - \phi_2 - \Delta(\phi_2 + 1 - \phi_1 - \Delta(\phi_1)))$$

Region 3:

$$\bar{\phi}_1 = \phi_1 + \Delta(\phi_1) - \Delta(1 - \phi_2 - \Delta(\phi_2 + 1 - \phi_1 - \Delta(\phi_1)))$$
$$\bar{\phi}_2 = \phi_2 + \Delta(\phi_2 + 1 - \phi_1 - \Delta(\phi_1))$$
$$- \Delta(1 - \phi_2 - \Delta(\phi_2 + 1 - \phi_1 - \Delta(\phi_1)))$$

Region 4:

$$\bar{\phi}_1 = \phi_1 + \Delta(\phi_1) + 1 - \Delta(1 - \phi_2)$$
$$\bar{\phi}_2 = \phi_2 - \Delta(1 - \phi_2)$$

Region 5:

$$\bar{\phi}_1 = \phi_1 + \Delta(\phi_1) - \Delta(1 - \phi_2)$$
$$- \Delta(2 - \phi_2 + \Delta(1 - \phi_2) - \Delta(\phi_2 - \phi_1 - \Delta(\phi_1)))$$
$$\bar{\phi}_2 = \phi_2 - 1 - \Delta(1 - \phi_2) + \Delta(\phi_2 - \phi_1 - \Delta(\phi_1))$$
$$- \Delta(2 - \phi_2 + \Delta(1 - \phi_2) - \Delta(\phi_2 - \phi_1 - \Delta(\phi_1)))$$

Region 6:

$$\bar{\phi}_1 = \phi_1 + \Delta(\phi_1) - \Delta(1 - \phi_2)$$
$$\bar{\phi}_2 = \phi_2 + \Delta(\phi_2 - \phi_1 - \Delta(\phi_1)) - \Delta(1 - \phi_2)$$

A.3 Dividing Curve Mappings

Curve 1:
$$\begin{aligned}
\bar{\phi}_1 &= \phi_1 + \Delta(\phi_1) \\
\bar{\phi}_2 &= 1
\end{aligned}$$

Curve 2:
$$\begin{aligned}
\bar{\phi}_1 &= \phi_2 + \Delta(\phi_2 + 1 - \phi_1 - \Delta(\phi_1)) \\
&\quad - \Delta(1 - \phi_2 - \Delta(\phi_2 + 1 - \phi_1 - \Delta(\phi_1))) \\
\bar{\phi}_2 &= 1
\end{aligned}$$

Curve 3:
$$\begin{aligned}
\bar{\phi}_1 &= \phi_2 - \Delta(1 - \phi_2) \\
\bar{\phi}_2 &= \phi_2 - \Delta(1 - \phi_2)
\end{aligned}$$

Curve 4:
$$\begin{aligned}
\bar{\phi}_1 &= 1 \\
\bar{\phi}_2 &= \phi_2 - \Delta(1 - \phi_2)
\end{aligned}$$

Curve 5:
$$\begin{aligned}
\bar{\phi}_1 &= \phi_1 + \Delta(\phi_1) - \Delta(1 - \phi_2) \\
\bar{\phi}_2 &= 1
\end{aligned}$$

A.4   Jacobian of Region 6

The explicit Jacobian for Region 6 of the Poincaré map is

$$\left[\begin{array}{cc} a_{11} & a_{12} \\ a_{21} & a_{22} \end{array}\right]$$

where

$$
\begin{aligned}
a_{11} &= 1 + 2\pi\varepsilon\cos\beta_1 \\
a_{12} &= 2\pi\varepsilon\cos\beta_2 \\
a_{21} &= -2\pi\varepsilon\cos\beta_3\left(2\pi\varepsilon\cos\beta_1 + 1\right) \\
a_{22} &= 2\pi\varepsilon\cos\beta_3 + 2\pi\cos\beta_2 + 1
\end{aligned}
$$

where

$$
\begin{aligned}
\beta_1 &= \left(2\pi\phi_1 + \frac{4\pi}{3}\right) \\
\beta_2 &= \left(\frac{4\pi}{3} - 2\pi(\phi_2 - 1)\right) \\
\beta_3 &= \left(\frac{4\pi}{3} - 2\pi\left(\phi_1 - \phi_2 + \pi\varepsilon\sin\left(\frac{4\pi}{3} + 2\pi\phi_1\right) + \varepsilon\frac{\sqrt{3}}{2}\right)\right)
\end{aligned}
$$

Appendix B

Algorithms

Given a uniform grid $\mathcal{G}$ and a (combinatorial) outer enclosure $\mathcal{F} : \mathcal{G} \rightrightarrows \mathcal{G}$ as defined in Section 4, we now give the definitions and algorithms used to compute isolating neighborhoods and index pairs in this project.

Definition B.0.1. *A* combinatorial trajectory *of a combinatorial enclosure $\mathcal{F}$ through $G \in \mathcal{G}$ is a bi-infinite sequence $\gamma_G = (\ldots, G_{-1}, G_0, G_1, \ldots)$ with $G_0 = G$, $G_n \in \mathcal{G}$, and $G_{n+1} \in \mathcal{F}(G_n)$ for all $n \in \mathbb{Z}$.*

Definition B.0.2. *The* combinatorial invariant set *in $\mathcal{N} \subset \mathcal{G}$ for a combinatorial enclosure $\mathcal{F}$ is*

$$\mathrm{Inv}(\mathcal{N}, \mathcal{F}) := \{G \in \mathcal{G} : \text{ there exists a trajectory } \gamma_G \subset \mathcal{N}\}.$$

Definition B.0.3. *The* combinatorial neighborhood *of $\mathcal{B} \subset \mathcal{G}$ is*

$$o(\mathcal{B}) := \{G \in \mathcal{G} : |G| \cap |\mathcal{B}| \neq \emptyset\}.$$

This set, $|o(\mathcal{B})|$, sometimes referred to as a *one box neighborhood of $\mathcal{B}$ in $\mathcal{G}$*, is the smallest representable neighborhood of $|B|$ in the grid $\mathcal{G}$.

Definition B.0.4. *If*
$$o(\mathrm{Inv}(\mathcal{N}, \mathcal{F})) \subset \mathcal{N}$$
then $\mathcal{N} \subset \mathcal{G}$ is a combinatorial isolating neighborhood *under $\mathcal{F}$.*

See [4] for the `grow_isolated` and `build_IP` algorithms. To execute these algorithms, we use CHomP [1].

Theorem B.0.5. *For $\mathcal{F} : \mathcal{G} \rightrightarrows \mathcal{G}$ a (combinatorial) outer enclosure on a uniform grid and combinatorial isolating neighborhood $\mathcal{N} \subset \mathcal{G}$ and combinatorial index pair $(\mathcal{P}_1, \mathcal{P}_0)$ produced by `grow_isolated` and `build_IP` algorithms respectively,*

1. $|\mathcal{N}|$ is an isolating neighborhood under f,

2. $P = (|\mathcal{P}_1, \mathcal{P}_0)$ is an index pair under f,

3. the output of CHomP is a sequence of matrix representatives for the shift equivalence classes of f_{P*} where $\mathrm{Con}(f, S) = [f_{P*}]_s$ and $S = \mathrm{Inv}(|\mathcal{N}|, f)$.